AGU PUBLICATIONS

Geophysical Research Letters

RESEARCH LETTER
10.1002/2014GL062126

Key Points:
- Novel array analysis for low-frequency radio waves
- Determination of wave number vector for VLF radio waves
- Novel approach to locating electromagnetic radiation from sprites

Correspondence to:
M. Füllekrug,
M.Fullekrug@bath.ac.uk

Citation:
Füllekrug, M., A. Mezentsev, R. Watson, S. Gaffet, I. Astin, and A. Evans (2014), Array analysis of electromagnetic radiation from radio transmitters for submarine communication, *Geophys. Res. Lett.*, *41*, 9143–9149, doi:10.1002/2014GL062126.

Received 5 OCT 2014
Accepted 18 NOV 2014
Accepted article online 25 NOV 2014
Published online 16 DEC 2014

Array analysis of electromagnetic radiation from radio transmitters for submarine communication

Martin Füllekrug[1], Andrew Mezentsev[1], Robert Watson[1], Stéphane Gaffet[2], Ivan Astin[1], and Adrian Evans[1]

[1]Centre for Space, Atmospheric and Oceanic Science, Department of Electronic and Electrical Engineering, University of Bath, Bath, UK, [2]Laboratoire Souterrain à Bas Bruit, UMS 3538, Université of Avignon, CNRS, Rustrel, France

Abstract The array analyses used for seismic and infrasound research are adapted and applied here to the electromagnetic radiation from radio transmitters for submarine communication. It is found that the array analysis enables a determination of the slowness and the arrival azimuth of the wave number vectors associated with the electromagnetic radiation. The array analysis is applied to measurements of ~20–24 kHz radio waves from transmitters for submarine communication with an array of 10 radio receivers distributed over an area of ~1 km × 1 km. The observed slowness of the observed wave number vectors range from ~2.7 ns/m to ~4.1 ns/m, and the deviations between the expected arrival azimuths and the observed arrival azimuths range from ~−9.7° to ~14.5°. The experimental results suggest that it is possible to determine the locations of radio sources from transient luminous events above thunderclouds with an array of radio receivers toward detailed investigations of the electromagnetic radiation from sprites.

1. Introduction

Recent theoretical model calculations predicted that the exponential growth and splitting of sprite streamers near ~40 km height cause electromagnetic radiation in the frequency range ~100 kHz [*Qin et al.*, 2012]. This prediction was promptly confirmed by experimental measurements of intense consecutive, or dancing, sprites [*Füllekrug et al.*, 2013b]. Similarly, sprite streamers near ~75 km height are the source of electromagnetic radiation in the frequency range <1 kHz [e.g., *Qin et al.*, 2012; *Cummer and Füllekrug*, 2001; *Pasko et al.*, 1998; *Cummer et al.*, 1998, and references therein]. It is hence somewhat surprising that sprites do not radiate significantly in the frequency range near 10 kHz [*Franz et al.*, 1990], which is possibly attributed to the relatively low streamer density of sprites near ~50–60 km height. On the other hand, recent electromagnetic radiation measurements during sprite occurrences, which are located only ~80 km away from a radio receiver, show a rapid succession of numerous broadband pulses with pausing time intervals ~50–100 μs [*Füllekrug et al.*, 2013a], similar to the pulse sequences observed during the initiation of lightning discharges [e.g., *Kolmasova et al.*, 2014; *Gurevich et al.*, 2013; *Stolzenburg et al.*, 2013, and references therein]. In fact, many sprites are associated with such pulse sequences, which blend into electromagnetic noise at large distances from the sprite [*Füllekrug et al.*, 2013b]. Yet the underlying wave number vectors required for a more detailed array analysis to locate sprites are not very well known.

Wave normal, or Poynting, vectors of electromagnetic waves are measured in space with three axis electric and magnetic field sensors [e.g., *Santolik et al.*, 2014, 2003]. At the surface of the Earth, it is not possible to use three axis electric or magnetic field measurements because the boundary conditions for electromagnetic fields near a conductor result in a screening of the vertical magnetic and horizontal electric fields and in a superposition with the electromagnetic fields induced inside the conductive Earth. As a result, this contribution aims to determine the wave number vectors by use of an array of radio receivers. Specifically, the array analyses developed for seismic and infrasound arrays [e.g., *Füllekrug et al.*, 2013c; *Rost and Thomas*, 2002; *Gaffet et al.*, 1998; *Cansi*, 1995] are adapted and subsequently exemplarily applied to ~20–24 kHz radio waves from radio transmitters for submarine communication to validate the array analysis.

2. Ansatz

An array of 10 radio receivers was deployed over an area of ~1 km × 1 km on an old airfield at Charmy Down near Bath in Southwest England [*Mezentsev and Füllekrug*, 2013]. The array is characterized by the sweet

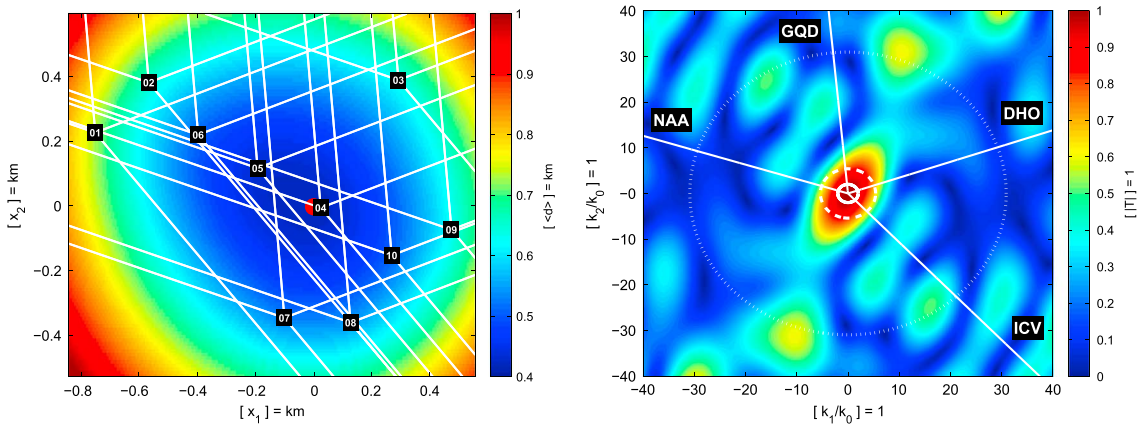

Figure 1. The array of radio receivers. (left) Ten radio receivers are distributed over an area of ~1 km × 1 km. The sweet spot of the array (red dot) minimizes the average distance <*d*> to all receivers. The radio waves of four transmitters sweep across the array from different directions (lines). (right) The array response (|T|) is most suitable for radio waves propagating along the north-west to south-east and the south-east to north-west direction as a result of the geometric distribution of the receivers. The Nyquist wave number (dotted circle) and the fundamental wave number (dashed circle) characterize the array. The wave numbers within the quasi-static part of the wave number spectrum are of interest (solid circle). The radio waves from the four transmitters Tavolara (ICV), Rhauderfehn (DHO), Skelton (GQD), and Cutler (NAA) arrive from different azimuths (lines).

spot (51.4277°N, 2.3429°W), i.e., the location with the smallest average distance ~419 m to all the radio receivers (Figure 1, left). The aperture of the array is defined by the geometry of the radio receiver locations that are constrained by logistic access to Charmy Down airfield. The measurements at the receivers $y_c(\boldsymbol{r}, t)$ are explained by an electromagnetic source field $E(t)$, which propagates as a plane wave $e^{-i(\mathbf{kr}-\omega t)}$ across the array of radio receivers

$$y_c(\mathbf{r_n}, t) = E(t)e^{-i(\mathbf{kr_n}-\omega t)}. \tag{1}$$

In this description, y_c is the complex trace that is composed of a real part and imaginary part, i.e., the originally recorded time series and the time series shifted by 90° [*Bracewell*, 1990, and references therein]. This ansatz enables a measurement of the envelope $|y_c|$ and the instantaneous phase φ_c when formulated in polar form $y_c = |y_c|e^{-i\varphi_c}$ [*Taner et al.*, 1979]. The complex trace depends on time t and on the receiver locations $\mathbf{r_n} = (x_{1,n}, x_{2,n})^T$ in the east-west (x_1) and north-south (x_2) directions with respect to the sweet spot of the network, where the receiver locations are numbered from $n = 1, 2, \ldots N = 10$. The electromagnetic source field $E(t)$ is composed of an amplitude $A(t)$ and phase $\phi(t)$ such that $E(t) = A(t)e^{-i\phi(t)}$ is independent of any receiver location. The wave number vector $\mathbf{k} = (k_1, k_2)^T$ lies in the horizontal $x_1 \times x_2$ plane because the array has no significant vertical gradient. The product ωt of the radio wave frequency ω and time t describes a continuous phase progression that is taken out of equation (1) by multiplication with $e^{-i\omega t}$ such that

$$y_n(t) = E(t)e^{-i\mathbf{kr_n}}. \tag{2}$$

This step ensures that the phase of $y_n(t)$ is referenced to the phase φ_0 at the start time of the recordings after the application of a low pass filter with a cutoff frequency of 150 Hz.

3. Array Aperture

The time independent array aperture or transfer function,

$$T(\mathbf{k}, \mathbf{r_n}) = \frac{1}{N}\sum_{n=1}^{N} e^{-i\mathbf{kr_n}} \tag{3}$$

describes the impulse response of the array with respect to the electromagnetic source field (Figure 1, right). This array transfer function is characterized by the Nyquist wave number k_N and the fundamental wave number k_F. The Nyquist wave number $k_N = 2\pi/(2d_{\min})$ is determined by the smallest distance $d_{\min} \approx 220.2$ m between two receivers in the array and the fundamental wave number $k_F = 2\pi/(2d_{\max})$ is determined by the largest distance $d_{\max} \approx 1261.4$ m between two receivers in the array. It is convenient to

Table 1. Properties of the Radio Communication Transmitters and Their Wave Normal Vectors[a]

Name	Call Sign	f (kHz)	Lat (deg)	Lng (deg)	d (km)	s (ns/m)	Φ_e (deg)	Φ_m (deg)	$\Delta\Phi$ (deg)
Tavolara, I	ICV	20.27	40.92°N	9.73°E	1490	4.13	−46.87	−52.08	5.21
Skelton, UK	GQD	22.10	54.73°N	2.88°W	370	2.65	95.41	92.87	2.54
Rhauderfehn, D	DHO	23.40	53.08°N	7.61°E	704	3.20	19.05	4.55	14.50
Cutler, Maine/US	NAA	24.00	44.65°N	67.28°W	4739	2.97	162.53	172.19	−9.66

[a]The radio transmitters for submarine communication are characterized by their call sign, center frequency f, geographic location *Lat*, *Lng*, and distance to the sweet spot of the array d. The wave normal vectors are characterized by the slowness s and the measured arrival azimuth Φ_m, which exhibits deviations $\Delta\Phi$ from the expected arrival azimuth Φ_e.

normalize the wave numbers k with the free space wave number $k_0 = \omega/c$, where ω is the frequency of the radio wave and c is the speed of light in vacuum such that $k_N/k_0 \approx 30.9$ and $k_F/k_0 \approx 5.4$ for a radio wave with a frequency of 22 kHz. However, this study is focused on the determination of relative wave numbers k/k_0 ranging from 0 to 2 in the quasi-static part of the wave number spectrum (Figure 1, right) to ensure that there is no ambiguity in the interpretation of the results.

4. Wave Number Vectors

The wave number vectors of the radio waves are determined by writing equation (2) in polar form

$$|y_n(t)|e^{-i\varphi_n(t)} = A(t)e^{-i\phi(t)}e^{-i\mathbf{k}\mathbf{r_n}} \tag{4}$$

and by arranging the phases into one equation for each of the receivers

$$(x_{1,n}, x_{2,n}, 1)\begin{pmatrix} k_1 \\ k_2 \\ \phi \end{pmatrix} = \varphi_n + \delta\varphi_n \quad \wedge \quad n = 1, 2, \ldots N = 10 \tag{5}$$

where the phase residuals $\delta\varphi_n$ need to be minimized. Equation (5) is an overdetermined linear system of equations that can be solved with the Gaussian method of least squares to obtain the best fitting solutions for k_1, k_2, and ϕ.

Four terrestrial radio transmitters for submarine communication are recorded with the array of radio receivers from 15:00:00 to 15:00:02 UTC on 13 May 2011 (Table 1). The wave number vectors are inferred by the use of equation (5). Subsequently, the wave number vectors are binned in a two-dimensional $k_1/k_0 \times k_2/k_0$ grid with a resolution $\Delta(k/k_0) = 0.01$. This distribution function exhibits four distinct maxima, which correspond to the wave number vectors of the four radio communication transmitters (Figure 2, left).

4.1. Horizontal Slowness

The length of the wave number vector $k = |\mathbf{k}|$ determines the apparent velocity $v_a = \omega/k$, which describes the radio wave propagation velocity as it appears to the array in a projection of the three-dimensional wave number vector onto the two dimensions of the array. The apparent velocity of the radio waves is often expressed in the corresponding horizontal slowness $s = 1/v_a$, which enables a convenient linear assessment of the travel time t_d of the radio wave across the array of receivers $t_d = sd$, where d is the distance traveled across the network. For example, an electromagnetic wave in vacuum has the slowness $s_0 = 1/c \approx 3.34$ ns/m. A larger slowness $s > s_0$ indicates an apparent velocity which is less than the speed of light, and a smaller slowness $s < s_0$ indicates that the radio wave arrives at the array from an elevation angle Θ. This elevation angle is determined by the ratio between the radio wave propagation speed in the medium near the array v_m and the apparent velocity v_a such that $\cos\Theta = v_m/v_a$, as inferred from a geometric analysis of the plane wave arriving at the array [*Rost and Thomas*, 2002, Figure 1]. The horizontal slowness of the radio waves from the four radio communication transmitters range from ~2.65 ns/m to ~4.13 ns/m (Table 1). These results show that the radio waves of the transmitters arrive from varying elevation angles that result from the distance-dependent superposition of the transverse electric and transverse magnetic radio wave propagation modes (TE_n/TM_n), possibly assisted by an influence of the geomagnetic field on the radio wave propagation.

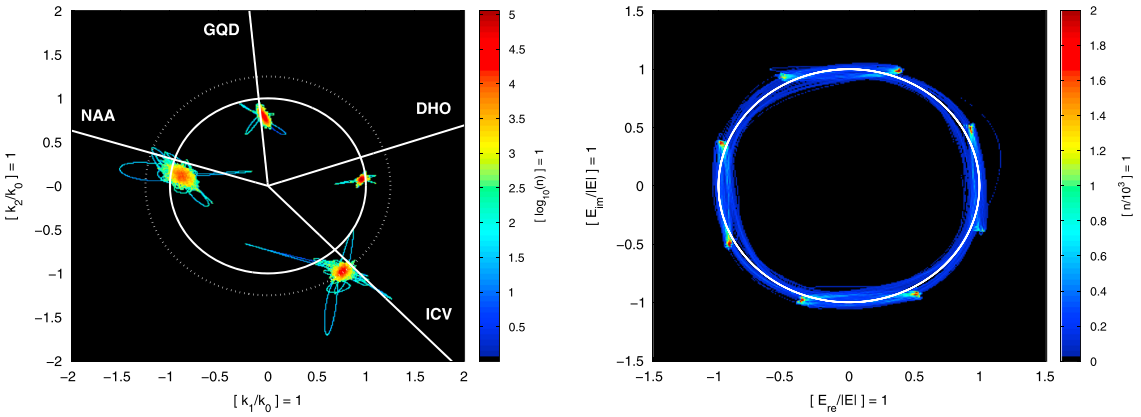

Figure 2. Distribution of wave number vectors and electromagnetic source fields. (left) The distribution of the normalized wave number vectors exhibits four distinct maxima. The maxima are located near the expected arrival azimuths of radio waves from the radio transmitters (solid lines) and near the unit circle (solid circle). All the maxima are located within a circle with radius $k/k_0 = 1.25$ (dashed circle). (right). The distribution of the electromagnetic source fields E from the transmitter in Rhauderfehn (DHO), Germany, exhibits eight clusters near the unit circle (solid circle) in the constellation diagram of the phase-modulated radio transmissions.

4.2. Arrival Azimuth

The orientation of the wave number vector reflects the arrival azimuth Φ of the radio wave, which is determined by the ratio between the east-west (k_1) and the north-south (k_2) component of the wave number vector such that $\Phi = \arctan(k_2/k_1)$. These arrival azimuths are measured with respect to the geographic east and compared to the expected arrival azimuths that are calculated assuming a propagation from the transmitters to the array along the great circle paths (Table 1). The expected arrival azimuths exhibit deviations from the measured arrival azimuths $\Delta\Phi$, which range from ~−9.7° to ~14.5° (Table 1). The observed deviations are indicative of an anisotropic wave propagation [e.g., *Füllekrug and Sukhorukov*, 1999], possibly as a result of the distance traveled at varying angles with the geomagnetic field [*Barr et al.*, 2000, and references therein].

5. Electromagnetic Source Field

The wave numbers can be used to determine the electromagnetic source field $E(t)$ from the recordings by rewriting equation (2)

$$e^{-i\mathbf{k}\,\mathbf{r_n}}E = y_n + \delta y_n \qquad \wedge \quad n = 1, 2, \ldots N = 10 \tag{6}$$

where the residuals of the measurements δy_n need to be minimized. Equation (6) is an overdetermined linear system of equations that can be solved with the complex Gaussian method of least squares, which results in a sparse spatial Fourier transform

$$E = \frac{1}{N}\sum_{n=1}^{N} y_n e^{i\mathbf{k}\,\mathbf{r_n}} \tag{7}$$

to determine the best fitting solution for the electromagnetic source field. It is convenient to normalize the electromagnetic source field $E(t)$ with the temporal average of its amplitude $< |E(t)| >$ such that $E(t)/< |E(t)| >$ describes relative changes of the amplitude and phase of the source field. The resulting normalized source field is binned on the complex plane with a resolution $\Delta(E/ < |E| >) = 0.01$. This distribution of the electromagnetic source field shows the constellation diagram of the phase modulated transmissions, e.g., for the transmissions from Rhauderfehn (Figure 2, right). The rotation of the constellation diagram with respect to the real and imaginary axes of the complex reference frame results from the fact that the phase is measured relative to the phase φ_0 at the start time of the recordings. The normalized source field is closely related to the coherency of the electromagnetic source field

$$E_c = \left| \frac{1}{N}\sum_{n=1}^{N} \frac{y_n e^{i\mathbf{k}\,\mathbf{r_n}}}{|y_n e^{i\mathbf{k}\,\mathbf{r_n}}|} \right| \tag{8}$$

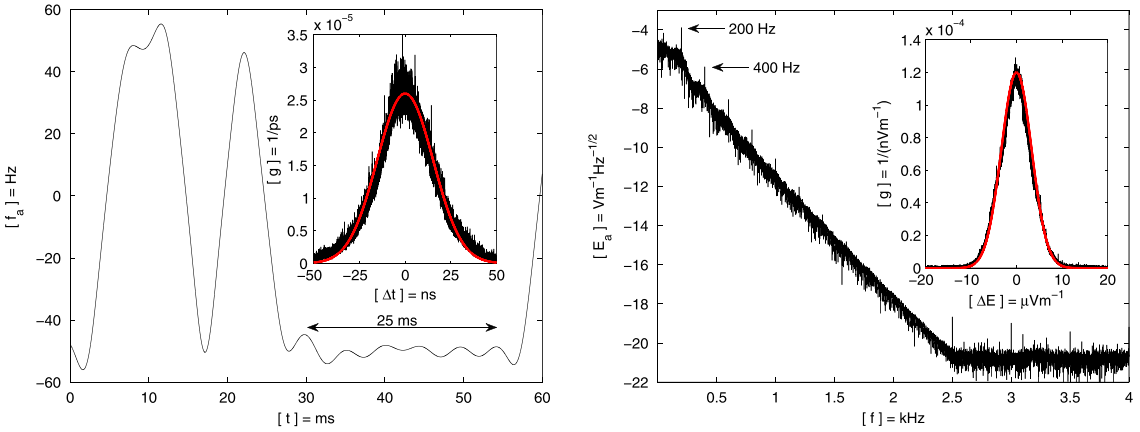

Figure 3. Properties of the electromagnetic source field. (left) The apparent frequency f_a changes between ±50 Hz and exhibits a repetition period of ~5 ms. The residuals of the phase determination follow a normal distribution function (red line) in excellent agreement with the accuracy of the radio receiver (inset figure). (right) The spectrum of the electromagnetic source field amplitude E_a extends up to 2.5 kHz and exhibits distinct peaks at 200 Hz with seven harmonics. The residuals of the electromagnetic source field determination follow a normal distribution function (red line) in excellent agreement with the accuracy of the radio receiver (inset figure).

which ranges between $0 \leq E_c \leq 1$ and measures the significance of the electromagnetic source field. The coherency can be used, for example, as a weight for phase coherent stacks to increase the signal-to-noise ratio of average electromagnetic source fields [*Schimmel and Paulssen*, 1997].

The phase modulation of the radio transmissions results in a deterministic phase progression which is conveniently expressed in the apparent frequency

$$\varphi = \omega_a t \quad \rightarrow \quad f_a = \frac{1}{2\pi}\frac{\mathrm{d}\varphi}{\mathrm{d}t} = \frac{1}{2\pi\Delta t}\frac{E_r\Delta E_i - E_i\Delta E_r}{|E|^2} \tag{9}$$

[*Taner et al.*, 1979] where E_r and E_i are the real and imaginary part of E (Figure 2, right) and Δt=1 μs is the sampling time interval of the recordings. The apparent frequency is measured relative to the center frequency of the transmission (Table 1) because it results from the temporal derivative of the phase in equation (9). This relative apparent frequency covers a total range of ~±50 Hz, and it exhibits distinct oscillations with a repetition period of ~5 ms (Figure 3, left), which is observed in the spectrum of $|E|$ as a spectral peak at 200 Hz with seven harmonics (Figure 3, right). Note that the spectral amplitudes of $|E|$ drop over many orders of magnitude down to the numerical limit of the spectral analysis.

6. Residuals

The residual phases $\delta\varphi_n$ are composed of two components. The first component is independent of time and frequency, and it is attributed to quasi-static clock offsets. The second component is not correlated between the receivers of the array, and it is attributed to the jitter of the clocks used at the individual receivers. The residual phases are expressed as temporal uncertainties $\delta t = \delta\varphi/\omega$ and follow a normal distribution function with a standard deviation ~15.3 ns (Figure 3, left, inset). The residuals of the electromagnetic source field δy_n are also composed of two components. The first component is independent of time and frequency, and it is attributed to the calibration of the receivers in the array. The second component is not correlated between the receivers of the array, and it is attributed to the quantization noise of the analogue-to-digital converters used at the individual receivers. The residuals follow a normal distribution function with a standard deviation ~3.3 μV/m (Figure 3, right, inset). The residual distributions for the time jitter and the quantization noise are in excellent agreement with the technical specifications of the radio receiver [*Füllekrug*, 2010, Figures 5 and 6]. This important result means that each sample of the measurements is explained by the wave number vector $(k_1, k_2)^T$, and the electromagnetic source field E with an accuracy down to the instrumental limits.

7. Discussion

In seismic and infrasonic array analysis, the elevation angles are determined from the wave propagation velocity in the medium v_m near the array that is not yet very well known for radio waves. This knowledge

could be gained by designing a volumetric, or three-dimensional, array to provide experimental evidence for the elevation angles, for example, by placing radio receivers on a self-configuring array of unmanned aerial vehicles, e.g., quadcopters, or by placing the array into a volcanic crater of suitable size. Alternatively, it might be possible to assess all the radio transmitters within the bandwidth of the radio receiver to determine a most likely, or minimum, wave propagation velocity in the medium near the array toward a determination of the elevation angles. Such a comprehensive assessment of all the elevation angles of electromagnetic radiation from known radio transmitters enables the opportunity to establish a standard reference map of the low-frequency radio sky, similar to known stellar constellations in radio astronomy. The main application of this reference map is to determine the relative location of electromagnetic radiation from radio sources above thunderclouds, such as sprites, gigantic jets, and possibly electron beams. For example, sprites are thought to cause impulsive radio noise associated with the growth and branching of individual streamers. The associated impulsive radio signals have a broad spectrum such that the array analysis to locate radio noise from sprites would use that part of the electromagnetic spectrum which is not occupied by known radio transmissions. The reference map will thereby enable a determination of the location of electromagnetic radiation from sprites relative to the known locations from radio transmitters. Another possibility to assess the radio noise from sprites is to slightly modify the array analysis to apply beam forming. Beam forming steers the antenna aperture toward the expected location of the electromagnetic radiation from sprites above thunderclouds to maximize the sensitivity of the array transfer function in that direction. This strategy requires a prediction of the propagation path of electromagnetic radiation from sprites which is well understood.

8. Summary

The data analysis concepts developed for seismic and infrasonic arrays are successfully adapted and applied to an array of radio receivers to infer the electromagnetic source fields and the wave number vectors of ~20–24 kHz radio waves from transmitters for submarine communication. The wave number vectors provide novel information on the horizontal slowness of the radio waves, which range from ~2.7 ns/m to ~4.1 ns/m depending on the arrival azimuths of the radio waves. It is expected that more extended array analyses will provide a wealth of novel insights into the physics of low-frequency radio waves, and possibly radio noise from sprites and yet unknown radio sources, with experiments that remain to be conducted in the future.

Acknowledgments

The work of M.F., A.M., and R.W. is sponsored by the Natural Environment Research Council (NERC) under grants NE/L012669/1 and NE/H024921/1. S.G. is supported by CNRS. The data used for this publication are available upon request from the communicating author. M.F. wishes to thank David Ll. Jones, Elisabeth Blanc. and Gerhard Müller for inspiration and encouragement to pursue this project.

The Editor thanks an anonymous reviewer for his/her assistance in evaluating this paper.

References

Barr, R., D. Jones, and C. Rodger (2000), ELF and VLF radio waves, *J. Atmos. Sol. Terr. Phys.*, *62*(17-18), 1689–1718, doi:10.1016/S1364-6826(00)00121-8.

Bracewell, R. (1990), Numerical transforms, *Science*, *248*(4956), 697–704, doi:10.1126/science.248.4956.697.

Cansi, Y. (1995), An automatic seismic event processing for detection and location: The P.M.C.C method, *Geophys. Res. Lett.*, *22*(9), 1021–1024, doi:10.1029/95GL00468.

Cummer, S., and M. Füllekrug (2001), Unusually intense continuing current in lightning produces delayed mesospheric breakdown, *Geophys. Res. Lett.*, *28*(3), 495–498, doi:10.1029/2000GL012214.

Cummer, S., U. Inan, T. Bell, and C. Barrington-Leigh (1998), ELF radiation produced by electrical currents in sprites, *Geophys. Res. Lett.*, *25*(8), 1281–1284, doi:10.1029/98GL50937.

Franz, R., R. Nemzek, and J. Winckler (1990), Television image of a large upward electrical discharge above a thunderstorm system, *Science*, *249*, 48–51, doi:10.1126/science.249.4964.48.

Füllekrug, M. (2010), Wideband digital low-frequency radio receiver, *Meas. Sci. Technol.*, *21*, 15901, doi:10.1088/0957-0233/21/1/015901.

Füllekrug, M., and A. Sukhorukov (1999), The contribution of anisotropic conductivity in the ionosphere to lightning flash bearing deviations in the ELF/ULF range, *Geophys. Res. Lett.*, *26*(8), 1109–1112, doi:10.1029/1999GL900174.

Füllekrug, M., A. Mezentsev, S. Soula, O. van der Velde, and A. Evans (2013a), Illumination of mesospheric irregularity by lightning discharge, *Geophys. Res. Lett.*, *40*, 6411–6416, doi:10.1002/2013GL058502.

Füllekrug, M., A. Mezentsev, S. Soula, O. van der Velde, and T. Farges (2013b), Sprites in low-frequency radio noise, *Geophys. Res. Lett.*, *40*, 2395–2399, doi:10.1002/grl.50408.

Füllekrug, M., et al. (2013c), Energetic charged particles above thunderclouds, *Surv. Geophys.*, *34*(1), 1–41, doi:10.1007/s10712-012-9205-z.

Gaffet, S., C. Larroque, A. Deschamps, and F. Tressols (1998), A dense array experiment for the observation of waveform perturbations, *Soil Dyn. Earthquake Eng.*, *17*(7-8), 475–484, doi:10.1029/1999GL900174.

Gurevich, A., et al. (2013), Correlation of radio and gamma emissions in lightning initiation, *Phys. Rev. Lett.*, *111*, 165,001, doi:10.1103/PhysRevLett.111.165001.

Kolmasova, I., O. Santolik, T. Farges, W. Rison, R. Lan, and L. Uhlir (2014), Properties of the unusually short pulse sequences occurring prior to the first strokes of negative cloud-to-ground lightning flashes, *Geophys. Res. Lett.*, *41*, 5316–5324, doi:10.1002/2014GL060913.

Mezentsev, A., and M. Füllekrug (2013), Mapping the radio sky with an interferometric network of low-frequency radio receivers, *J. Geophys. Res. Atmos.*, *118*, 8390–8398, doi:10.1002/jgrd.50671.

Pasko, V., U. Inan, T. Bell, and S. Reising (1998), Mechanism of ELF radiation from sprites, *Geophys. Res. Lett.*, *25*(18), 3493–3496, doi:10.1029/98GL02631.

Qin, J., S. Celestin, and V. Pasko (2012), Low-frequency electromagnetic radiation from sprite streamers, *Geophys. Res. Lett.*, *39*, L22803, doi:10.1029/2012GL053991.

Rost, S., and C. Thomas (2002), Array seismology: Methods and applications, *Rev. Geophys.*, *40*(3), 1008, doi:10.1029/2000RG000100.

Santolik, O., M. Parrot, and F. Lefeuvre (2003), Singular value decomposition methods for wave propagation analysis, *Radio Sci.*, *38*(1), 1010, doi:10.1029/2000RS002523.

Santolik, O., C. Kletzing, W. Kurth, G. Hospodarsky, and S. Bounds (2014), Fine structure of large-amplitude chorus wave packets, *Geophys. Res. Lett.*, *41*, 239–299, doi:10.1002/2013GL058889.

Schimmel, M., and H. Paulssen (1997), Noise reduction and detection of weak, coherent signals through phase-weighted stacks, *Geophys. J. Int.*, *130*, 497–505, doi:10.1111/j.1365-246X.1997.tb05664.x.

Stolzenburg, M., T. Marshall, S. Karunarathne, N. Karunarathna, L. Vickers, T. Warner, R. Orville, and H.-D. Betz (2013), Luminosity of initial breakdown in lightning, *J. Geophys. Res. Atmos.*, *118*, 2918–2937, doi:10.1002/jgrd.50276.

Taner, M., F. Koehler, and R. Sheriff (1979), Complex seismic trace analysis, *Geophysics*, *44*(36), 1041–1063, doi:10.1190/1.1440994.